Available online at www.sciencedirect.com

ScienceDirect

Energy Procedia 80 (2015) 72 – 82

Energy Procedia

12th Deep Sea Offshore Wind R&D Conference, EERA DeepWind'2015

Modelling and analysis of CIGRE HVDC offshore multi-terminal benchmark grid

Jordi Pegueroles[a]*, Mike Barnes[b], Oriol Gomis[a], Antony Beddard[b] and Fernando D. Bianchi[a]

[a]*Catalonian Institue for Energy Research (IREC), 08930, Barcelona, Spain*
[b]*School of Electrical & Electronic Enineering, University of Manchester, Manchester, United Kingdom*

Abstract

HVDC power transmission systems are being commissioned in the North Sea to link inland power grids with large offshore wind power farms. The growing number of large wind farms is driving the need to design more reliable high power transportation systems, leading to the conception of multi-terminal HVDC grids. These future grids will be purely formed by power electronics converters, the control of which will have to be designed to ensure proper performance and robust operation. This paper presents the analysis of the benchmark system proposed by the CIGRE working group SC B4, focusing on the proper selection of the components models and parameters. The small signal model of the system is first formulated. Then the bandwidth of the different control loops is obtained and the fidelity of the HVDC line model is selected accordingly. Finally, the performance of the benchmark system is studied by means of small signal analysis and compared numerical time series simulation of the non-linear model.

Peer-review under responsibility of SINTEF Energi AS

Keywords: offshore HVDC; Small Signal Analysis; Multi-Terminal;

* Corresponding author. Tel.: +34 933 562 615; fax: + 34 933 563 802.
E-mail address: jpegueroles@irec.cat

Peer-review under responsibility of SINTEF Energi AS
doi:10.1016/j.egypro.2015.11.409

1. Introduction

New power transmission systems will be required to connect multiple wind farms located far offshore with onshore connection points. High voltage direct current (HVDC) technology [1] is the main candidate for implementing these new power transmission systems, forming a multi-terminal HVDC (MT-HVDC) grid. Towards the implementation of such systems, the CIGRE SC B4 working group has proposed the use modular multi-level converters (MMC) with overhead lines and undersea DC cables [2].

In a MT-HVDC system [3], the operation of every converter may be reflected to each node of the system, leading to interactions among power converters, and interactions between converters and transmission lines [4]. The analysis of VSC-HVDC with different control parameters and structures has been performed in [5], using a small signal model of the converter. Also, the impact of current controlled DC choppers in MT-HVDC systems has been studied in [6], by using detailed numerical simulation.

This paper analyses the stability margins of the control scheme proposed in [2], by means of small signal studies using accurately linearised models of the different elements in a multi-terminal HVDC system. The stability results are compared with a numerical simulation of the non-linear model of the system implemented in SIMULINK/SimPowerSystems.

2. Modelling

The system under study is a four-terminal symmetric monopole (±200 kV) MT-HVDC system, as illustrated in Fig. 2. It connects the offshore wind power plant at F1 and an offshore oil platform at E1 to the onshore nodes B3 and B2, this last one located further inland (labelling of converters is derived from [2]). This benchmark system consists of long overhead lines and cables in series, and HVDC-MMC power converters, in order to study interactions among these elements.

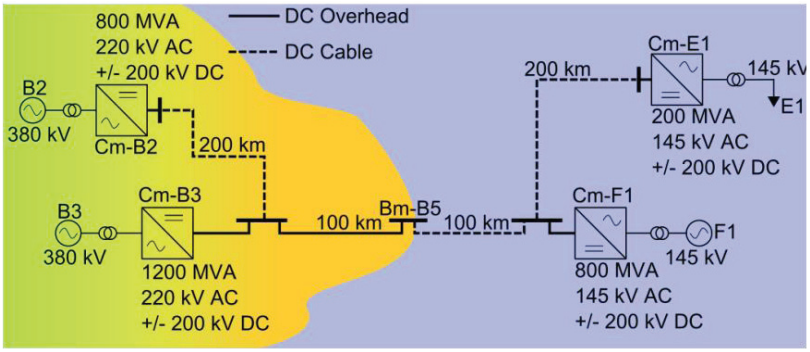

Fig. 1. Benchmark DC system proposed by CIGRE.

The power converters forming the benchmark system have different control objectives. On the one hand, onshore converters, Cm-B2 and Cm-B3, are converters regulating AC power with droop control of the DC voltage. The droop control modifies the external power set-point of the converter in order to maintain the DC voltage within the operational range (1 ± 0.15 pu). On the other hand, the offshore converters have different control objectives. Converter Cm-F1 accepts the power drawn from the wind farm, and implements a dead-band control of the DC voltage. This is to manage extreme cases; *e.g.* a fault on the AC side blocking the operation of the droop converters. Finally, the converter Cm-E1 supplies the power demand of the oil platform. This converter does not actively contribute to the DC voltage regulation.

Different regulatory specifications for the power converters may exist depending on the country hosting the power stations. However, some minimum operational requirements are shared in those regulations. As a guideline, some typical requirements are defined in [7], requiring the power converter station operate under difference

adverse grid conditions, such as variations of the grid frequency and voltage. Moreover, according to [7], the converter must remain stable and connected to the system without tripping for a close-up solid three-phase or any unbalanced short circuit fault for up to 140 ms; *i.e.* it must have fault ride-through capability.

2.1. Control of a HVDC converter

To fulfill the aforementioned requirements and achieve the control objectives of each converter, the CIGRE SC B4 working group has proposed a benchmark control scheme for each case.

2.1.1. Power Control

The typical control objective of MT-HVDC power converters is to track an AC power set-point, commonly given by the on-shore transmission system operator (TSO). To accomplish this end, the control scheme depicted in Fig. 2 is proposed by CIGRE.

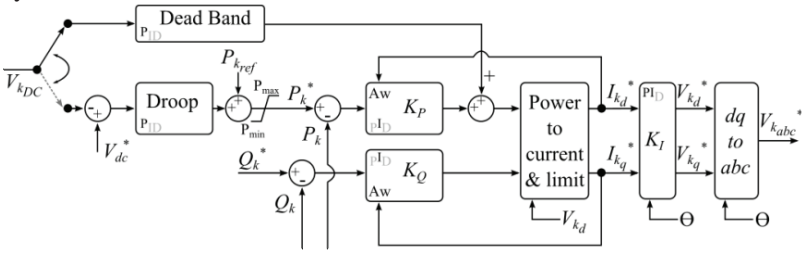

Fig. 2. Control scheme of a HVDC converter.

The proposed control scheme relies on a cascaded structure, where the droop control modifies the power reference of the active power control, and the active and reactive power control outputs are the references to the low level current control, which generates the voltage reference for the MMC. In this scheme, the dead band control does not modify the power control reference (as the droop control would), but modifies the power control output. This scheme is valid for both droop and dead-band control, but both controls cannot be active simultaneously. The droop control can be expressed as

$$\begin{aligned} \hat{P}_k^* &= P_{k_{ref}} + K_{k_{dr}}\left(V_{DC}^* - V_{k_{DC}}\right) \\ P_k^* &= \mathrm{sat}\left(\hat{P}_k^*,\ P_{k_{max}},\ P_{k_{min}}\right),\ k \in \aleph \end{aligned} \quad (1)$$

$$\text{where } \mathrm{sat}(a, MAX, MIN) = \begin{cases} MAX & if \quad a \geq MAX \\ a & if \quad MAX > a > MIN \\ MIN & if \quad MIN \leq a \end{cases},$$

and $\aleph$={B2, B3, F1, E1}, $K_{k_{dr}}$ is the droop gain, $V_{k_{DC}}$ is the DC voltage of converter k, $P_{k_{ref}}$ is the power set-point of the converter, V_{DC}^* is the nominal voltage of the HVDC grid, and P_k^* is the reference of the power control. From herein and for the sake of clarity, it is assumed that, $k \in \aleph$ unless otherwise stated.

2.1.2. AC voltage Control

In addition to active and reactive power control as in Fig. 2, MMC-HVDC converters might provide AC voltage regulation when they are used to either supply isolated electrical systems or when connected to weak AC systems. For these situations, CIGRE proposes a voltage control scheme to regulate the electrical grid and provide the necessary power demand, shown in Fig. 3. It should be noted that this scheme does not provide any means to limit the current when the converter is overloaded neither does it provide any support, active or passive, to the DC grid.

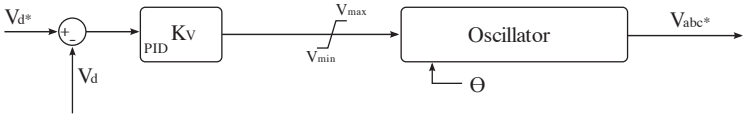

Fig.3. Control scheme of a HVDC converter in AC voltage control mode.

Converter Cm-E1 uses this control scheme to supply the demand of the offshore oil platform. It is assumed that this can be approximated in the small signal analysis as a constant power control, neglecting the dynamics of the load, in order to simplify the analysis.

2.2. Component model

In this paper, two different models are considered for the analysis of the CIGRE benchmark system. On the one hand, non-linear detailed models are used to implement a numerical simulation using SIMULINK Simpowersystems. On the other hand, linearised models of the electrical components such as the power transmission lines, the HVDC converters, the multi-terminal DC grid, and the AC side dynamics are used for the small signal analysis of the system. This subsection describes how to obtain the small signal models. It should be noted that all variables are expressed in the per unit (pu) system.

2.2.1. Modular Multi-level Converter model

The power converter is modeled using an average-value model (AVM) based on switching functions, which approximates the system dynamics by neglecting switching details, *i.e.* insulated gate bipolar transistors (IGBT) are not explicitly represented. The AVM assumes that all internal variables of the MMC are perfectly controlled, all sub-modules capacitors balanced and harmonic currents circulating in each leg are suppressed. The modeling is based on guidelines of [8]; the following equations describe the MMC voltage for each phase

$$V_{kj}^{c} = sat\left(V_{kj}^{*}, V_{k_{DC}}/2\,, -V_{k_{DC}}/2\right), \qquad \forall\, j = a,b,c$$

where V_{kj}^{c} is the j-phase voltage at the output of the converter k, V_{kj}^{*} is the voltage reference for the MMC. For the small signal analysis it is assumed that the MMC is working in the linear region. In the DQ reference frame, the small signal voltages can be expressed as

$$\Delta V_{k_{dq}}^{c} = \Delta V_{k_{dq}}^{*}. \tag{2}$$

The MMC controllers used in the detailed numerical simulation has been implemented in the discrete form, using a zero order sample and hold sampled at the switching frequency for the measurements of the continuous time signals. The AC voltage waveform is generated using a zero order sample and hold of the V_{kj}^{c} signal, using a nearest level control (NLC) modulation in order to emulate switching of the sub-modules, *i.e.* the output AC voltage is a staircase waveform. The DC side of the model (see Fig. 4) is derived using the principle of power balance, where the power injected to the DC side is the power drawn from the AC side minus the power losses of the MMC. Current losses are calculated as

$$I_{k_{loss}} = R_{k_{loss}} \hat{I}_{k_{DC}}^{2} / V_{k_{DC}}\,, \tag{3}$$

with $\hat{I}_{k_{DC}}$ given by

$$\hat{I}_{k_{DC}} = \frac{P_{k_{AC}}}{V_{k_{DC}}}, \tag{4}$$

where $P_{k_{AC}}$ is the active power of the MMC k and $R_{k_{loss}}$ is the equivalent resistance of the MMC. Thus, the DC current injected to the equivalent capacitor C_{k_e} of the MMC is

$$I_{k_{DC}}^{c} = \hat{I}_{k_{DC}} - \hat{I}_{k_{loss}}. \tag{5}$$

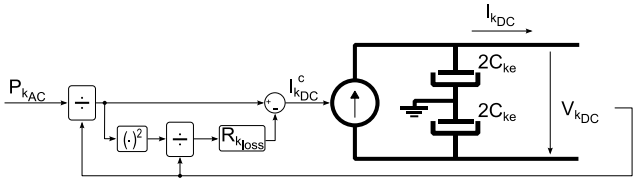

Fig. 4. DC side model of the MMC.

In order to obtain the small signal model of (5), equations (3) and (4) are linearised, obtaining

$$\Delta I^{c}_{k_{DC}} = \left(\frac{1}{\overline{V_{k_{DC}}}} + 2R_{k_{loss}}\,\overline{P_{k_{AC}}}\right)\Delta P_{k_{AC}} - \left(\frac{\overline{P_{k_{AC}}}}{\overline{V^{2}_{k_{DC}}}} + 3\frac{R_{k_{loss}}\overline{P_{k_{AC}}}}{V^{4}_{k_{DC}}}\right)\Delta V_{k_{DC}}, \tag{6}$$

where the over-line denotes the equilibrium values in steady state, and Δ the small signal variables.

2.2.2. Line model

When the frequency spectrum of the signals involved in the simulation is not too wide, the assumption of frequency-independent line parameters constitutes a reasonable simplification. In such cases, cascading T circuits is a simple alternative to obtain a state space description of the power transmission line [9]. Fig. 5 shows a power HVDC transmission line represented by connecting short nominal T sections in cascade.

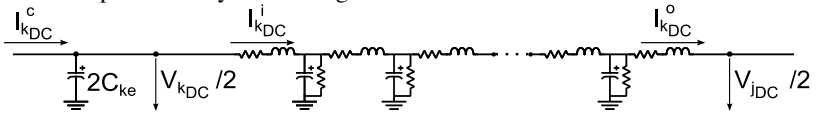

Fig. 5. Line model used for linearisation.

The number of sections to be used depends on the frequency range of concern. In this study, the frequency range will be determined by the bandwidth of the droop control, which is the system interacting with the power HVDC line. A good approximation of the highest frequency range represented by the cascaded nominal circuits is given by the following equation

$$f_{max} = \frac{N}{\pi\,\Gamma\,\sqrt{LC}},$$

where L and C are the inductance and capacitance per length unit respectively, N is the number of sections and Γ is the line length. The resulting linear model of the line can be expressed in the state-space as

$$\frac{d}{dt}x_{line} = \Lambda_{line}x_{line} + B_{line}\Delta V_{line},\ \Delta I_{line} = C_{line}x_{line}, \tag{7}$$

With $x_{line} = [\, i^{1}_{dc}\ v^{1}_{dc}\ i^{2}_{dc}\ v^{2}_{dc} \ldots\ i^{2N+1}_{dc}\,]^{T}$, Λ defined in the appendix, and

$$r = \Gamma\frac{R}{N+1}, \qquad l = \Gamma\frac{L}{N+1}, \qquad c = \Gamma\frac{C}{N}, \qquad g = \Gamma\frac{G}{N},$$

where R, L, C, G are the resistance, inductance, capacitance and conductance per length unit respectively. Let $\Delta I_k = Y_{k\to j}\,\Delta V_k$ denote the transfer function from the voltage at node k to the current drawn at node k; *i.e.* $B_{line} = \left[\frac{1}{l}\ 0 \ldots\ 0\right]^{T}$ and $C_{line} = [1\ 0 \ldots\ 0]$. Likewise, let $\Delta I_j = Y_{k\to j}\,\Delta V_k$ denote the transfer function from the voltage at node k to the current injected at node j; *i.e.* $B_{line} = \left[\frac{1}{l}\ 0 \ldots\ 0\right]^{T}$ and $C_{line} = [0\ 0 \ldots\ 0\ 1]$.

2.2.3. DC grid

The former line models (7) are used to form a multiple input multiple output (MIMO) system for analysing the small signal multi-terminal system. To form the MIMO system, first it is required to write the nodal admittance matrix as (8), where ΔI_k and ΔV_k are the DC current injected in every node and the node voltage respectively; $Y_{k\leftrightarrow l}$, $k \neq l$ are the admittance line models as defined in (7).

$$\begin{bmatrix}\Delta I_{B2_{DC}}\\ \Delta I_{B3_{DC}}\\ \Delta I_{F1_{DC}}\\ \Delta I_{E1_{DC}}\end{bmatrix} = \begin{bmatrix} Y_{B2\to B3} & -Y_{B3\to B2} & 0 & 0\\ -Y_{B2\to B3} & Y_{B3\to B2}+Y_{B3\to F1} & -Y_{F1\to B3} & 0\\ 0 & -Y_{B3\to F1} & Y_{F1\to E1} & -Y_{E1\to F1}\\ 0 & 0 & -Y_{F1\to E1} & Y_{E1\to F1}\end{bmatrix}\begin{bmatrix}\Delta V_{B2_{DC}}\\ \Delta V_{B3_{DC}}\\ \Delta V_{F1_{DC}}\\ \Delta V_{E1_{DC}}\end{bmatrix} \tag{8}$$

2.2.4. AC grid

The AC grid model is composed by the output impedance of the converter's arms and the series impedance of the interfacing ΔY transformer. This modelling is possible since the measurements of the AC signals (voltage and current) are taken on the primary side of the transformer, connected to the AC grid. The output impedance of the converter and the transformer can be expressed in the DQ reference frame as

$$\frac{d}{dt}x_{ac} = \Lambda_{ac}\, x_{ac} + \left[\frac{1}{L_{lg}+L_{tr}}\right]^T \Delta V_{k_d}^c,\ \Lambda_{ac} = \begin{bmatrix} -\frac{R_{lg}+R_{tr}}{L_{lg}+L_{tr}} & \omega \\ -\omega & -\frac{R_{lg}+R_{tr}}{L_{lg}+L_{tr}} \end{bmatrix}, \tag{9}$$

with

$$x_{ac} = \left[\Delta I_{k_d}^c \Delta I_{k_q}^c\right]^T, \quad \begin{bmatrix}\Delta P_{k_{AC}} \\ \Delta Q_{k_{AC}}\end{bmatrix} = \begin{bmatrix} \frac{3\overline{V_{k_d}}}{2} & \frac{3\overline{V_{k_q}}}{2} \\ \frac{3\overline{V_{k_q}}}{2} & -\frac{3\overline{V_{k_d}}}{2} \end{bmatrix}\begin{bmatrix}\Delta I_{k_d}^c \\ \Delta I_{k_q}^c\end{bmatrix} + \begin{bmatrix} \frac{3\overline{I_{k_d}}}{2} & \frac{3\overline{I_{k_q}}}{2} \\ \frac{3\overline{I_{k_q}}}{2} & -\frac{3\overline{I_{k_d}}}{2} \end{bmatrix}\begin{bmatrix}\Delta V_{k_d} \\ \Delta V_{k_q}\end{bmatrix},$$

where $\Delta V_{k_{dq}}$ is the AC grid voltage, L_{lg}, L_{tr}, R_{lg}, R_{tr} are the inductance and resistance of the MMC arm and transformer respectively, ω is the AC grid frequency and $\Delta I_{k_{dq}}^c$ are the converter output AC currents in the DQ reference frame.

3. Small signal multi-terminal system

In order to form the complete small signal model, in this section the relations among the models of the components defined in the previous section will be formulated.

3.1. AC dynamics of converter k

To obtain the transfer function from $\Delta P_{k_{AC}}^*$ to $\Delta P_{k_{AC}}$, first the closed loop transfer function of the current control and the AC side dynamics can be obtained. The current control loop, as proposed in [2], is a PI control with a decoupling feed-forward term, which can be expressed as a state space system

$$\frac{d}{dt}x_{k_{PI}^c} = \begin{bmatrix} ki_c & 0 \\ 0 & ki_c \end{bmatrix}\begin{bmatrix}\Delta I_{k_d}^* - \Delta I_{k_d}^c \\ \Delta I_{k_q}^* - \Delta I_{k_q}^c\end{bmatrix},$$

$$\begin{bmatrix}\Delta V_{k_d}^* \\ \Delta V_{k_q}^*\end{bmatrix} = x_{k_{PI}^c}\begin{bmatrix} kp_c & 0 \\ 0 & kp_c \end{bmatrix}\begin{bmatrix}\Delta I_{k_d}^* \\ \Delta I_{k_q}^*\end{bmatrix} + \begin{bmatrix}\Delta V_{k_d} \\ \Delta V_{k_q}\end{bmatrix} - \begin{bmatrix} kp_c & (L_{lg}+l_{tr})\omega \\ (L_{lg}+l_{tr})\omega & kp_c \end{bmatrix}\begin{bmatrix}\Delta I_{k_d}^c \\ \Delta I_{k_q}^c\end{bmatrix} \tag{10}$$

where kp_c and ki_c are the control parameters, and $x_{k_{PI}}^c$ are the integrator states. The small signal power control can be expressed as a state space system as well

$$\frac{d}{dt}x_{k_I^P} = \begin{bmatrix} ki_p & 0 \\ 0 & ki_p \end{bmatrix}\begin{bmatrix}\Delta P_{k_{AC}}^* - \Delta P_{k_{AC}} \\ \Delta Q_{k_{AC}}^* - \Delta Q_{k_{AC}}\end{bmatrix},\ \begin{bmatrix}\Delta I_{k_d}^* \\ \Delta I_{k_q}^*\end{bmatrix} = \frac{1}{\overline{V_{k_d}}}x_{k_P^p} + \frac{\overline{P_{k_{AC}}}}{\overline{V_{k_{DC}}^2}}\begin{bmatrix}\Delta V_{k_d} \\ \Delta V_{k_q}\end{bmatrix}, \tag{11}$$

where ki_p is the power control tuning parameter, and $x_{k_I^p}$ is the integrator state. Using (2), (9), (10) and (11) it is straight forward to form the closed loop transfer function from $\Delta P_{k_{AC}}^*$ to $\Delta P_{k_{AC}}$, denoted as *G-AC*$_k$, which can be expressed as

$$x_{ac}^{cl} = \Lambda_{ac}^{cl}\, x_{ac}^{cl} + \left[0 \ldots 0\ ki_p\ 0\right]^T \Delta P_{k_{AC}}^*,\ \Delta P_{k_{AC}} = \left[\frac{3}{2}\overline{V_{k_d}}\ \ \frac{3}{2}\overline{V_{k_q}}\ \ 0\ \ldots 0\right] x_{ac}^{cl} \tag{12}$$

with Λ_{ac}^{cl} defined in the appendix.

where $x_{ac}^{cl} = \left[\Delta I_{k_d}^c\ \Delta I_{k_q}^c\ \ x_{k_{PI}^c}\ \ x_{k_I^p}\right]^T$, and R_{ac} and L_{ac} are the sum of the converter arm and transformer resistance and inductance respectively.

3.1.1. Dynamics with dead band control

The dead band control constitutes a non-linear feedback of the DC voltage injected to the current reference. It can be expressed as

$$I_{k_{db}} = \begin{cases} -K_{db}\left(V_{DC} - V_{DC_{db}}^{MAX}\right) & if \quad V_{DC} > V_{DC_{db}}^{MAX} \\ -K_{db}\left(V_{DC} - V_{DC_{db}}^{MIN}\right) & if \quad V_{DC} < V_{DC_{db}}^{MIN} \\ 0 & else \end{cases},$$

where K_{db} is the dead band control gain, the input of the d-axis of the current control is $I_{k_{db}} + I_{k_d}^*$, and $V_{DC_{db}}^{MAX}$ and $V_{DC_{db}}^{MIN}$ are the limits of the dead band region. The linearised model with dead band control can be expressed as

$$x_{ac}^{cl} = \Lambda_{ac}^{cl}\, x_{ac}^{cl} + B_{ac}^{cl}\left[\Delta P_{k_{AC}}^{*}\ \Delta V_{k_{DC}}\right]^T, \tag{13}$$

$$B_{ac}^{cl} = \begin{bmatrix} 0 & 0 & 0 & 0 & ki_p & 0 \\ -kp_c K_{db} & 0 & -ki_c K_{db} & 0 & 0 & 0 \end{bmatrix}, \quad \Delta P_{k_{AC}} = \left[\tfrac{3}{2}\overline{V_{k_d}} \ \ \tfrac{3}{2}\overline{V_{k_q}} \ \ 0 \ \ldots \ \ 0\right] x_{ac}^{cl}$$

in the appropriate region of operation of V_{DC}.

3.1.2. DC dynamics of converter k

DC dynamics are defined as the transfer function from $\Delta P_{k_{AC}}$ to $\Delta V_{k_{DC}}$. To obtain this transfer function, the voltage can be expressed as a function of the current difference

$$\Delta V_{k_{DC}} = \frac{1}{sC_{k_e}}\left(\Delta I_{k_{DC}}^{c} - \Delta I_{k_{DC}}\right). \tag{14}$$

Replacing (6) in (14) and after some simple manipulations, it can be obtained

$$\Delta V_{k_{DC}} = \frac{1}{sC_{k_e}}\left(\Upsilon \Delta P_{k_{AC}} - \Delta I_{k_{DC}}\right),\ \Upsilon = \frac{\frac{1}{\overline{V_{k_{DC}}}} + 2R_{k_{loss}}\overline{P_{k_{AC}}}}{1 + \frac{1}{sC_{k_e}}\left(\frac{\overline{P_{k_{ac}}}}{\overline{V_{k_{DC}}^2}} + \frac{3R_{k_{loss}}\overline{P_{k_{AC}}}}{\overline{V_{k_{DC}}^4}}\right)} \tag{15}$$

3.2. Complete closed loop dynamics

Using the previously defined models, the interconnected closed loop system can be build as shown in Fig. 6. The blocks VSC $_{B2, B3, E1, F1}$ are formed by the transfer function defined in (15); blocks G-AC$_{B2, B3, E1, F1}$ are either transfer functions (12) or (13); DC GRID block is defined in (8).

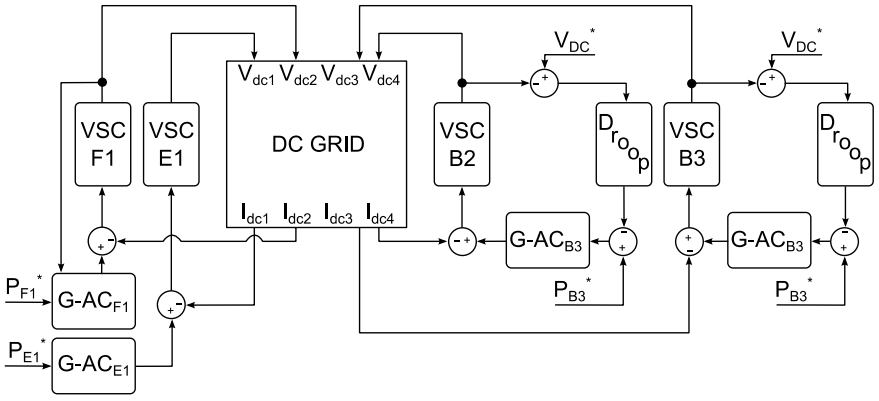

Fig. 6. Small signal model of the multiterminal system.

4. Results

In this section, the performance of the MT-HVDC benchmark system proposed in [2] will be analysed. The small signal analysis results will be compared with the results of a numerical simulation of the detailed system implemented in MATLAB/Simulink and Simpowersystems toolbox.

Firstly, the frequency behaviour of the HVDC cable is presented in Fig. 7. The model is a state space representation with 11 states obtained by selecting $N = 5$ in (7), with the parameters summarized in Table 1. The bode plot of the 200 km DC cable linking Cm-B2 and Cm-B3 is shown in Fig. 7. The model with CIGRE paramters is accurate up to 130~Hz approximately, enough for the frequency range of analysis of this paper.

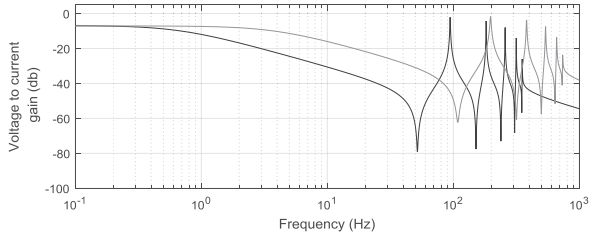

Fig. 7. Cable model comparison with CIGRE values (black) and proposed values (gray)

Table 1. Cable parameters used in the model.

	CIGRE	Used values	
Resistance	0.0110	0.0113	Ω/km
Inductance	2.6150	0.4660	mH/km
Capacitance	0.2185	0.2800	μF/km
Conductance	0.0550	0.0550	S/km

As it can be seen, the response of the DC cable presents a resonance at 94~Hz, with the parameters from [2]. However, studies in the line model parameters indicates that other, slightly modified, parameters might be more appropriate in this case. The key difference between the two sets of parameters is that inductance value employed for this work is smaller since it is based on a VSC-HVDC system with a metallic return. With the used values, the resonance is displaced at a frequency of 197.5~Hz, as observed in the light gray line in Fig. 7. Since the interaction among converters is given by the droop control, the dead band control and the DC cables, the bandwidth of these controls loops is obtained by analysing the sigma values of the multi-variable system. Fig. 8 shows the closed loop sigma values, which indicate the bandwidth is approximately 10~Hz. As the DC cable model is accurate up to 10 times this frequency, this model is valid for the analysis.

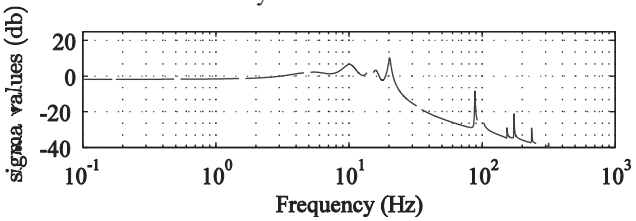

Fig. 8. Maximum sigma values of the closed loop system during normal operation.

Fig. 9 shows the closed loop sigma values when converter Cm-F1 is in the dead band control mode. The dead band control modifies the current reference of the AC current loop, achieving a wider control bandwidth than the droop control. As shown by the sigma values, this bandwidth is approximately 40 Hz, still under the frequency resolution of the cable model.

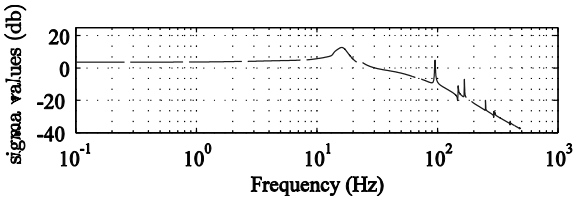

Fig. 9. Maximum sigma values of the closed loop system with dead band control operation.

To analyse the performance of the benchmark model, two different scenarios are studied: a) converter Cm-F1 AC side trips permanently due to a fault on the offshore AC grid; b) converter Cm-B3 AC side is disconnected as a result of a permanent fault in the AC onshore grid. In both scenarios the initials conditions are identical, $P_{B2_{AC}} = 400$ MW, $P_{B3_{AC}} = -800$ MW, $P_{F1_{AC}} = 500$ MW, $P_{B2_{AC}} = -100$ MW (minus sign indicates the power is injected to the AC grid).

The small signal analysis indicates that the system with two droop control converters presents a faster response than the system with only one droop converter. However, when two droop controls are working in parallel, the transient response of the system to some disturbances, such as the loss of a converter or an AC voltage sag, has a much higher overshoot. This behavior can be observed by the pole location shown at Fig. 10. Scenario a) and b) correspond to fig. 10a and fig. 10b respectively.

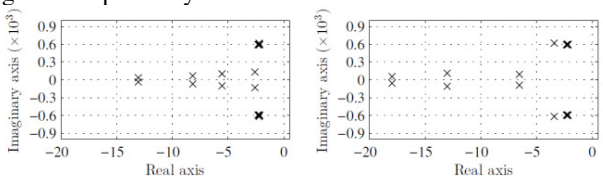

(a) With AC side of Cm-F1 converter blocked.

(b) With AC side of Cm-B3 converter blocked.

Fig. 10. CIGRE four terminal benchmark system poles.

Table 2. Modes from the CIGRE four terminal benchmark system; With AC side of Cm-F1 blocked

Pole	Damping	Frequency (Hz)
-2.39E+01	1.00E+00	3.80
-3.27E+01	1.00E+00	5.20
-3.28E+01	1.00E+00	5.23
-2.39E+01	1.00E+00	5.92
-1.31E+01 ± 3.48e+01i	3.51E-01	11.05
-8.18E+00 ± 6.89e+01i	1.18E-01	16.01
-5.55E+00 ± 1.00e+02i	5.52E-02	20.86
-2.59E+00 ± 1.31e+02i	1.98E-02	49.53

Table 3. Modes from the CIGRE four terminal benchmark system; With AC side of Cm-B3 blocked

Pole	Damping	Frequency (Hz)
-2.39E+01	1.00E+00	4.18
-3.27E+01	1.00E+00	5.21
-1.80E+01 ± 5.67E+01i	3.02E-01	9.46
-6.54E+00 ± 9.18E+01i	7.11E-02	14.64
-9.29E+01	1.00E+00	14.79
-1.30E+01 ± 1.11E+02i	1.17E-01	17.72
-2.02E+02 ± 2.37E+02i	6.49E-01	49.53
-1.98E+02 ± 2.88E+02i	5.67E-01	55.57

The time responses of the system in scenarios a) and b) are shown in fig. 11 and fig. 12 respectively. As it can be seen in Fig. 11, the interaction of the droop control results in a oscillatory response of the system when the converter Cm-F1 trips (t = 3.2 s). The overshoot of the DC voltage in terminals F1 and E1 due to the effect of the droop control over the HVDC transmission line is particularly noteworthy.

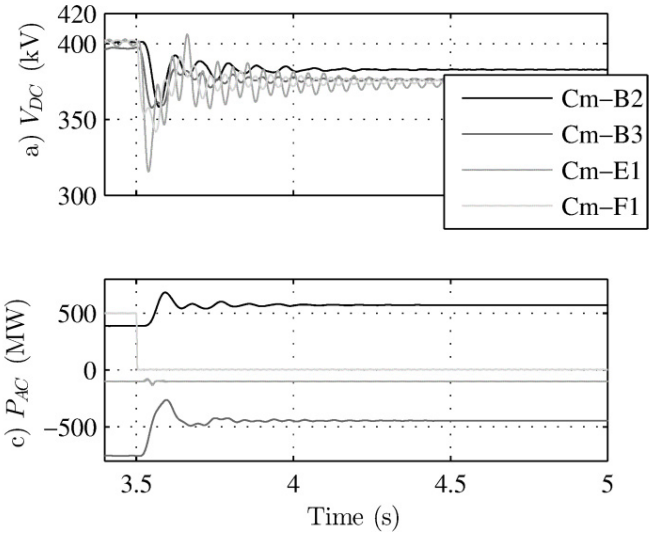

Fig. 11. Response upon the loss of Cm-F1; 2 Droop controllers.

In the scenario b), where the converter Cm-B3 is lost, the small signal analysis indicates that the oscillations in the DC voltage ought to be extinguished faster than in scenario a). This is corroborated by the time domain simulation performed, with the time response of the system upon the loss of converter Cm-B3 at t = 3.5 s shown in Fig. 12. This faster response is due to the non-interaction between the droop control loops, and also due to the fast action of the dead band control.

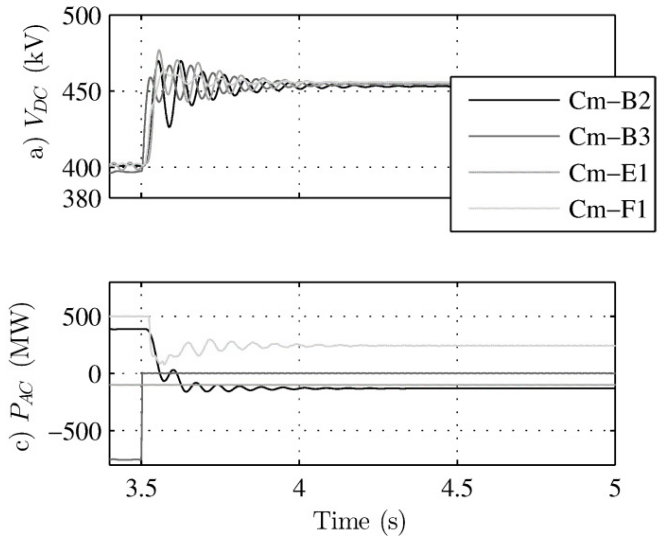

Fig. 12. Response upon the loss of Cm-B3; only one droop controller.

5. Conclusions

Careful coordination between droop controllers for MT-HVDC is required, since parallel operation of DC voltage controllers result in an oscillatory response. In the modelling of MT-HVDC systems, the model of the cable must be chosen with care to match the frequency range of interest of any study. As a result of the small signal analysis, it can be concluded that the design of a more sophisticated control scheme for the droop control might be required to improve the performance of the power transmission system, especially to reduce the oscillations on the DC voltage.

References

[1] C. Osauskas and A. Wood, Small-signal dynamic modeling of HVDC systems, Pow.Deliv. IEEE Trans. on, vol.18, no.1, pp.220–225, 2003.
[2] CIGRE Working Group B4 57, Guide for the Development of HVDC Grid, 2014.
[3] A. M. Alsseid, D. Jovcic, and A. Starkey, "Small signal modelling and stability analysis of multiterminal vsc-hvdc," in Power Electronics and Applications (EPE 2011), Proceedings of the 2011-14th European Conference on. IEEE, 2011, pp. 1–10.
[4] C. Karawita and U. Annakkage, "Multi-infeed hvdc interaction studies using small-signal stability assessment," Power Delivery, IEEE Transactions on, vol. 24, no. 2, pp. 910–918, April 2009.
[5] W. Wang, A. Beddard, M. Barnes, and O. Marjanovic, "Analysis of active power control for VSC-HVDC," Power Delivery, IEEE Transactions on, vol. 29, no. 4, pp. 1978–1988, Aug 2014.
[6] M. Mohammadi, M. Avendano-Mora, M. Barnes, and J. Chan, "A study on fault ride-through of VSC-connected offshore wind farms," in Power and Energy Society General Meeting (PES), 2013 IEEE, July 2013, pp. 1–5.
[7] National Grid Electricity Transmission, The Grid Code, 2014, issue 5 Rev.1.
[8] H. Saad, J. Peralta, S. Dennetiere, J. Mahseredjian, J. Jatskevich, J. Martinez, A. Davoudi, M. Saeedifard, V. Sood, X. Wang et al., "Dynamic averaged and simplified models for mmc-based hvdc transmission systems," Power Delivery, IEEE Transactions on, vol. 28, no. 3, pp. 1723–1730, 2013.
[9] J. A. R. Macías, A. Gomez Exposito, and A. Bachiller Soler, "A comparison of techniques for state-space transient analysis of transmission lines," Power Delivery, IEEE Transactions on, vol. 20, no. 2, pp. 894–903, 2005.

Appendix

$$\Lambda = \begin{bmatrix} -r/l & 1/l & 0 & 0 & 0 & \cdots & 0 \\ -1/c & -g/c & 1/c & 0 & 0 & \cdots & 0 \\ 0 & -1/l & -r/l & 1/l & 0 & \cdots & 0 \\ 0 & 0 & -1/c & -g/c & 1/c & \cdots & 0 \\ \vdots & \vdots & \vdots & \ddots & \ddots & \ddots & 0 \\ 0 & 0 & 0 & 0 & 0 & -1/l & -r/l \end{bmatrix}$$

$$\Lambda_{\mathrm{ac}}^{\mathrm{cl}} = \begin{bmatrix} -\frac{R_{ac}+kp_c}{L_{ac}} & 0 & \frac{1}{L_{ac}} & 0 & \frac{kp_c}{\overline{V_{k_d}}} & 0 \\ 0 & -\frac{R_{ac}+kp_c}{L_{ac}} & 0 & \frac{1}{L_{ac}} & 0 & \frac{kp_c}{\overline{V_{k_d}}} \\ -ki_c & 0 & 0 & 0 & \frac{ki_c}{\overline{V_{k_d}}} & 0 \\ -\frac{3}{2}\overline{V_{k_d}} & -\frac{3}{2}\overline{V_{k_q}} & 0 & 0 & 0 & 0 \\ -\frac{3}{2}\overline{V_{k_q}} & \frac{3}{2}\overline{V_{k_d}} & 0 & 0 & 0 & 0 \end{bmatrix}$$